Influence of Alloying Elements on the Kinetics of Massive Transformation in Gamma Titanium Aluminides

U. PRASAD and M.C. CHATURVEDI

The effect of alloying elements, Nb and Mn on massive transformation in Ti-45Al based alloys was studied. The alloy samples were heat treated at 1350 °C for 30 minutes and subsequently cooled to room temperature by furnace cooling, air cooling, and water quenching. The microstructural evolution in various alloys was investigated by a detailed microstructural characterization of the heat-treated samples by optical, scanning, and transmission electron microscopy. It was observed that the volume fraction of the massively transformed gamma in water-quenched samples increased from nil in the Mn-free alloy to ~70 pct in the alloy containing 2 at. pct Mn. Nb had a minimal effect on the extent of transformation. The effects of Nb and Mn have been rationalized on the basis of the site occupancy of the alloying elements and their possible influence on the phase boundaries and grain size. An attempt has also been made to elucidate the mechanism of massive transformation in these alloys. Based on the results obtained, the influence of Mn and Nb on the kinetics of massive transformation is presented and discussed and, the CCT diagrams for different alloys used in this study are proposed.

I. INTRODUCTION

TIAL-based two-phase titanium aluminide alloys have long been considered to be suitable candidates for high-temperature structural applications, mainly because of their high specific strength and modulus, and good high-temperature strength retention properties.[1–5] Unfortunately, these attractive properties are invariably accompanied by low room-temperature ductility and fracture toughness, and this restricts the usage of these alloys. Various efforts have been and are being made to overcome these drawbacks, to enhance the effective use of these alloys. A number of alloys of engineering importance based on Ti-(45-48)Al, with an appropriate combination of ternary and quaternary alloying elements (Cr, Mn, V, Nb, Ta, etc.), have been identified and developed through intensive research over the past two decades. These are two-phase alloys containing α_2 and γ phases. The proportion and morphology of the constituent phases in the microstructure can be varied significantly by altering the composition of the alloy and their processing techniques. The mechanical properties are strongly dependent on microstructure, and an optimum balance of all the mechanical properties can be achieved by controlling the proportion of different phases and also by controlling the grain size. The microstructural modifications can be brought about by varying the alloy chemistry and alloy processing and by thermal and thermomechanical treatments.

Numerous modes of phase transformations have been identified in the Ti-Al system during various heat treatments. The $\alpha \rightarrow \gamma_m$ massive-type transformation is among one of the major transformations in TiAl alloys. This was first observed in the Ti-Al system by Wang *et al.*[6,7] in 1992. They reported the formation of massive γ-phase (γ_m) in a Ti-48Al alloy when the alloy was cooled from the α-phase field at cooling rates sufficiently high to suppress the formation of lamellar ($\alpha_2 + \gamma$) microstructure. Since then, this transformation has been reported in a number of TiAl-based alloys.[6–20] Attempts have been made to enhance the understanding of the kinetics, thermodynamics, and mechanism of the massive transformation as applied to the Ti-Al system, based on the defect structure and the nature of product/parent interphase interfaces.[8,15,17,18] However, no consensus exists regarding these issues. Several aspects of the $\alpha \rightarrow \gamma_m$ massive-type transformation are still not fully comprehended, specifically, the reaction start temperatures for different alloys, driving force for the transformation, and growth kinetics and their mechanisms. Limited information is available on the effect of composition on these aspects of massive transformation.

The purpose of the present investigation was to study the effect of alloying elements, namely, Nb and Mn, on massive transformation in TiAl alloys. Ti-45Al based alloys with different concentrations of Nb and Mn were used in this investigation. The alloy samples were heated at 1350 °C (α-phase field) and subsequently cooled to room temperature at various rates. The experimental details and the results obtained in this investigation are discussed in the sections that follow. Based on the experimental observations and microstructural characterization, the effect of Nb and Mn on kinetics of the massive transformation has been elucidated and schematic CCT diagrams have been proposed for the alloys used in this investigation. An attempt has been also made to consider the mechanism of massive transformation based on the microstructural features of water-quenched samples.

U. PRASAD, Postdoctoral Fellow, and M.C. CHATURVEDI, Professor and Canada Research Chair, are with the Department of Mechanical Engineering, University of Manitoba, Winnipeg, MB, Canada R3T 5V6. Contact e-mail: mchat@cc.umanitoba.ca

This article is based on a presentation made in the symposium entitled "Fundamentals of Structural Intermetallics," presented at the 2002 TMS Annual Meeting, February 21–27, 2002, in Seattle, Washington, under the auspices of the ASM and TMS Joint Committee on Mechanical Behavior of Materials.

II. EXPERIMENTAL DETAILS

A. *Alloy Composition and Starting Microstructures*

Four different TiAl-based alloys with nominal compositions of Ti-45Al-2Nb-2Mn (alloy I), Ti-45Al-2Nb-0.4Mn (alloy II), Ti-45Al-2Nb (alloy III), and Ti-45Al (alloy IV) (all compositions in at. pct) were used in this study. Alloys I and II were prepared by Howmet Corporation (USA) by casting and hot-isostatic pressing ("hipping") at 1250 °C and 172 MPa for 4 hours and were supplied in the form of 10 to 12-mm thick slabs. Alloys III and IV were prepared at the University of Birmingham (Birmingham, United Kingdom) by plasma arc melting and casting followed by hipping at 1250 °C and 172 MPa for 4 hours. The alloys were supplied in the form of buttons weighing about 1 kg. The actual measured chemical composition of the alloys, along with their oxygen concentrations, are given in Table I. Figure 1[21] shows the binary Ti-Al phase diagram used as a reference in this study. The composition marked in this phase diagram corresponds to the Al concentration of the alloys used. As seen, the alloys lie in the $\alpha + \gamma$ two-phase field and the expected microstructure in this composition range is fully lamellar. This microstructure was indeed observed in the as-received alloys (Figures 2(a) through (d)). The actual lamellar colony size of the as-received samples could not be determined, as the colony boundaries could not be defined very well.

B. *Sample Preparation and Heat Treatment*

Specimens, 10 × 7 × 5 mm in dimension, were cut by electric discharge machining (EDM) from the slabs of alloys I and II. Specimens from the buttons of alloys III and IV, ~10 to 12 × 6 × 6 mm in size, were machined by EDM. They were then cleaned with ethyl alcohol in an ultrasonic bath and then encapsulated in vycor evacuated to $\sim 10^{-6}$ Torr and subsequently back-filled with commercial purity argon to a pressure of 140 Torr. The encapsulated samples were annealed at 1350 °C (α-phase field) for 30 minutes and subsequently cooled to room temperature by furnace cooling (FC), air cooling (AC), and water quenching (WQ). Cooling rates were measured using a National Instruments (Texas, USA) data acquisition system. Figure 3 shows a schematic line diagram representing the experimental setup used for cooling rate measurements. The cooling rates corresponding to furnace cooling, air cooling, and water quenching were measured to be 2 °C/min to 3 °C/min, 25 °C/s, and ~1000 °C/s, respectively.

Table I. Actual Measured Compositions of the Alloys

Alloys	Compositions, At. Pct				Oxygen (ppm)
	Al	Nb	Mn	Ti	
Alloy I	45.16	2.06	1.72	balance	650
Alloy II	44.9	2.15	0.4	balance	510
Alloy III	45.2	1.85	—	balance	550
Alloy IV	45.5	—	—	balance	450

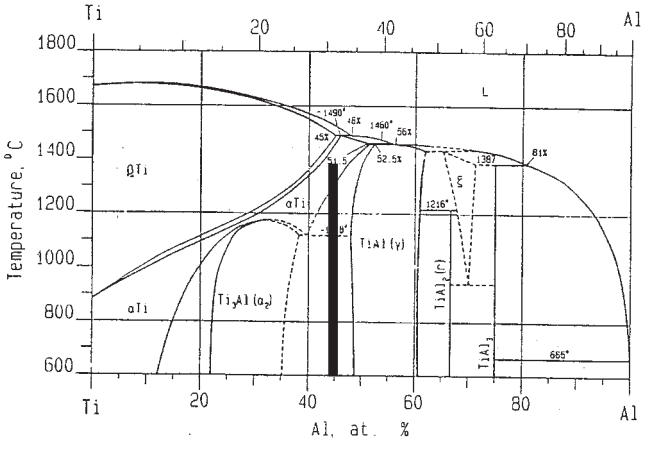

Fig. 1—Binary Ti-Al phase diagram.[21] The composition marked corresponds to the Al concentration of the alloys used in this study.

C. *Microstructural Characterization*

The samples for optical metallography were prepared by standard metallographic techniques and etched by a modified Kroll's reagent (7 pct HF, 21 pct HNO_3, and 72 pct H_2O). An inverted reflected-light microscope equipped with a CLEMEX* vision 3.0 image analysis system was used for qualitative and quantitative optical metallography. The volume fraction of different phases in the microstructure was determined based on the difference in gray level. A JSM-5900LV scanning electron microscope, equipped with an Oxford (Oxford Instruments, UK) energy dispersive spectrometer (EDS) and Inca analyzing software were used for the examination of the polished cross-section samples.

*CLEMEX is a trademark of Clemex Technologies Inc., Longuevil, Canada.

Thin foils were prepared to characterize the microstructure of bulk and subsurface layer of the heat-treated samples by transmission electron microscopy (TEM). For this purpose, 0.5-mm-thick slices were cut from the cross section of the specimens by EDM. These were then reduced to ~100 μm in thickness using 600-grit abrasive paper. The 3 mm-diameter discs were punched out by EDM and were further thinned using a twin-jet polishing unit. The electrolyte used for electropolishing was a solution of 5 pct perchloric acid, 30 pct butan-1-ol, and 65 pct methanol. Polishing was carried out at −30 °C to −35 °C and at 30 to 32 V. The thin foils were examined in a JEOL*-2000FX transmission electron microscope/scanning transmission electron microscope operated at 200 kV.

*JEOL is a trademark of Japan Electron Optics Ltd., Tokyo.

III. RESULTS AND DISCUSSION

A. *Furnace-Cooled Microstructures*

Figures 4(a) through (d) show the microstructures of the FC samples. As seen in these figures, annealing the alloy samples at 1350 °C for 30 minutes followed by furnace cooling to room temperature resulted in a complete decomposition of the high-temperature alpha phase and in the formation of fully lamellar microstructures in alloys, I, II, III, and IV. However, the average lamellar colony size varied with

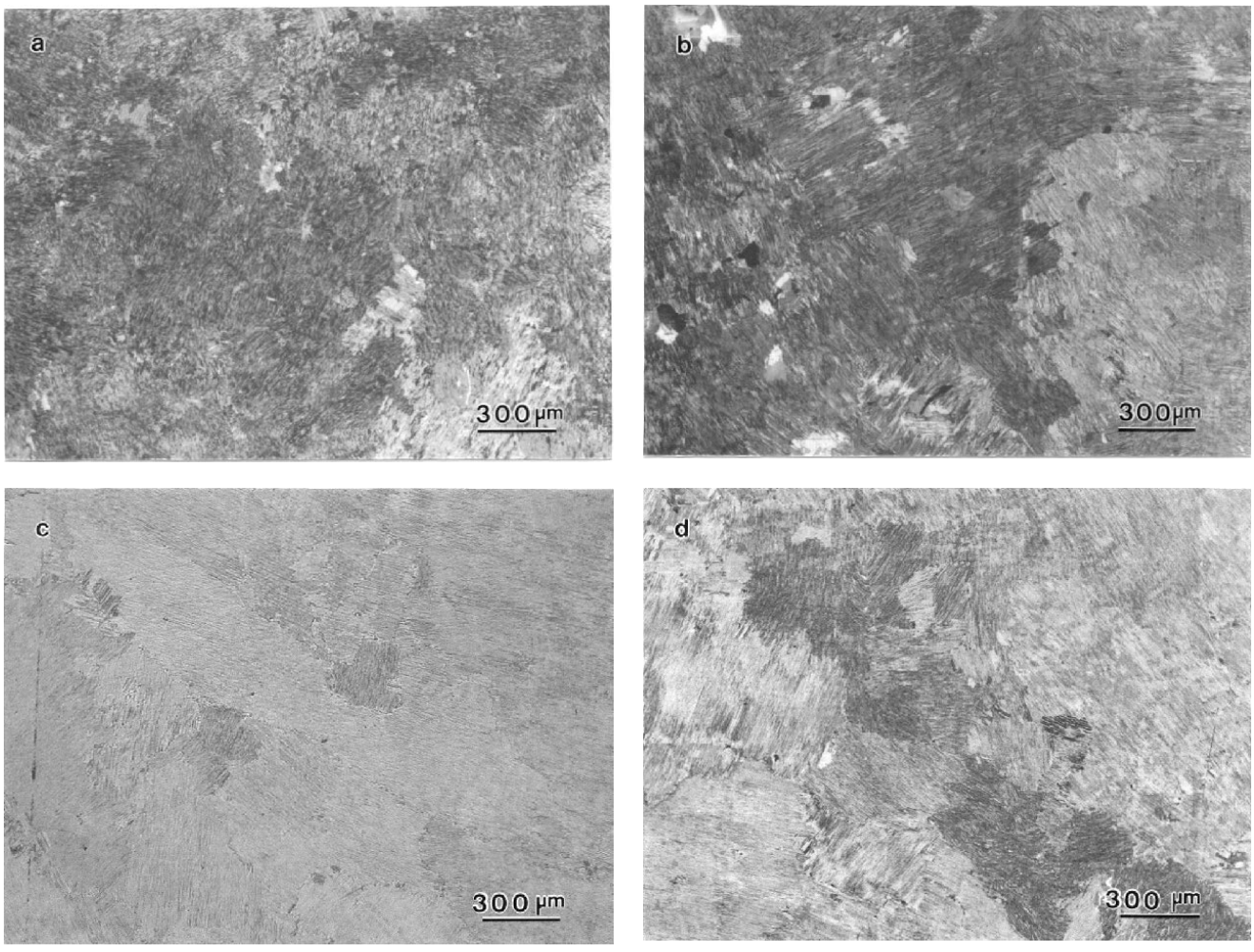

Fig. 2—As-received microstructure of (*a*) alloy I (Ti-45Al-2Nb-2Mn), (*b*) alloy II (Ti-45Al-2Nb-0.4Mn), (*c*) alloy III (Ti-45Al-2Nb), and (*d*) alloy IV (Ti-45Al).

the Mn concentration in the alloy, with the smallest grain size (colony size) obtained in alloy I (2 at. pct Mn). The ternary alloy (III) exhibited the largest grain size. Table II lists the average grain size of the FC samples as a function of alloy composition.

B. *Microstructural Characterization of Air-Cooled Samples*

Air cooling of alloy I (45-2-2) to room temperature after annealing at 1350 °C for 30 minutes resulted in the formation of a relatively fine lamellar microstructure with dark patches, as shown in Figure 5. Figure 6(a) is a TEM bright-field image of the air-cooled sample that shows the presence of the single-phase region along with the lamellar microstructure. Figures 6(b) and (c) show selected area diffraction patterns (SADPs) corresponding to the [111] and [101] zone axes of gamma phase. Figure 6(d) is a dark-field image confirming the presence of gamma phase along with a lamellar region. The dark patches in Figure 6(a) therefore were identified to be of gamma phase.

Air cooling of alloy II (45-2-04) caused a massive-type transformation. As shown in Figure 7, the microstructure consisted mainly of dark-etched regions with very small amounts of white regions ($V_f \sim 100$ pct). The TEM analysis of the thin foils confirmed the presence of massively transformed gamma (γ_m) in the air-cooled sample (Figures 8(a) through (d)). Air cooling thus corresponds to the critical cooling rate for massive transformation in alloy II. This suggests that the critical cooling rate for massive transformation in alloy II is lower than that in alloy I.

Increasing the cooling rate of alloy III (45-2-0) to air cooling resulted in a microstructure consisting primarily of alpha-2 phase with some dark patches of massively transformed gamma regions near the grain boundaries ($V_f \sim 8$ pct) (Figure 9). However, no γ_m grains could be observed in the thin regions of TEM foils because of a very low percentage of the transformation product present in the microstructure.

Air cooling of alloy IV (45-0-0) resulted in a microstructure consisting of fine lamellae with relatively planar grain boundaries (Figure 10). The grain size (lamellar colony size) was observed to be the same as that observed in the FC samples. Also observed was the occasional presence of dark patches of gamma phase near the grain boundaries, which were identified to be massively transformed gamma phase, as will be shown later. The volume fraction of this phase was approximately 5 pct. The TEM analysis confirmed the dark phase to be massively transformed gamma phase (Figures 11(a) and (b)). The gamma phase was also

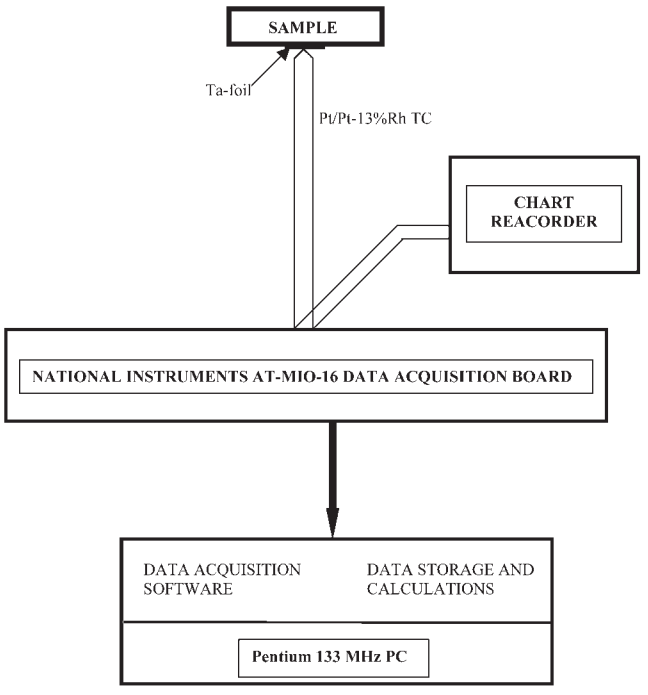

Fig. 3—Block diagram of the experimental setup used to measure cooling rates.

found to be present along the grain boundaries (Figure 11(e)), suggesting that γ_m nucleates at the grain boundaries and subsequently propagates into the neighboring grains, when the conditions are favorable. Comparing the microstructures of AC samples of alloys III and IV suggests that Nb suppresses lamellar structure formation, thus decreasing the critical cooling rate for massive transformation.

C. *Microstructural Characterization of Water-Quenched Samples*

Effect of alloying elements on the rate of massive transformation was investigated by water quenching the specimens. Water quenching of alloy I (45-2-2) to room temperature after annealing at 1350 °C for 30 minutes resulted in a microstructure that consisted primarily of massively transformed gamma (dark-etched regions) and patches of α_2 phase (white regions), as shown in Figure 12(a). Higher-magnification imaging of the sample indicated the presence of the γ_m phase at grain boundaries as well as inside the prior α grains (Figure 12(b)). This suggested that nucleation of massively transformed gamma seemingly takes place both at the prior grain boundaries as well as at some energetically favorable locations within the grains. However, in order to positively establish that γ_m nucleates intragranularly, a detailed TEM analysis and three-dimensional imaging of the microstructure is required. As seen from Figure 12(a), the $\alpha \rightarrow \gamma_m$ transformation was only partially suppressed by the $\alpha \rightarrow \alpha_2$ ordering reaction. The volume fraction of massively transformed gamma phase was measured to be ~70 pct. Figure 13(a) shows a SADP corresponding to the $[110]_\gamma$ zone axis. Figures 13(b) and (c) show a pair of TEM bright-field and dark-field images confirming the presence of massively transformed gamma phase in the water-quenched sample. The overall microstructure consisted of large patches of cluster of γ_m grains along with α_2 phase, as shown in the collage in Figure 14. Backscattered electron (BSE) imaging of the polished cross section of the water-quenched sample (Figure 15) showed a weak composition contrast between the two phases. The chemical composition of α_2 and γ_m phase, measured by EDS, is given in Table III. As seen, there was no significant difference in the compositions of the two product phases, except for the slightly higher Al and Mn concentrations in γ_m phase. The Nb did not show any preferential partitioning between the two phases. The average atomic numbers of the α_2 and γ_m phases were 18.38 and 18.34, respectively. This difference in the average atomic numbers of the two phases is not significant enough to cause the contrast observed in Figure 15. Also, it does not seem like an orientation effect as the contrast would have changed in different orientations if it were the case. On the contrary, γ_m always appeared dark and α_2 always appeared white in BSE imaging. The weak contrast in the BSE image, therefore, is more likely to be a combination of composition and topographic contrast.

Water quenching of alloy II (45-2-0.4) also resulted in suppression of the massive transformation by the competing $\alpha \rightarrow \alpha_2$ ordering reaction. The microstructure consisted of occasional patches (dark region) of massive gamma in a featureless matrix of α_2 phase (Figure 16a). The volume fraction of massively transformed gamma was measured to be ~25 pct. The composition of α_2 and γ_m phases, measured by EDS, is given in Table III. It was again observed that there was no significant difference in the composition of the two product phases, except for slightly higher Mn and Al concentrations in γ_m. Nb did not partition between α_2 and γ_m.

Water quenching of alloy III to room temperature after annealing at 1350 °C for 30 minutes, on the other hand, resulted in a microstructure that consisted entirely of α_2 phase (Figure 16(b)). The composition remained unchanged and the alloy underwent a simple $\alpha \rightarrow \alpha_2$ ordering reaction. Lastly, water quenching of alloy IV resulted in a partial suppression of the massive transformation by the competing $\alpha \rightarrow \alpha_2$ ordering reaction. The resulting microstructure (Figure 16(c)) consisted of 8 to 10 pct γ_m in α_2 matrix.

D. *Analysis of the Effect of Mn and Nb on Massive Transformation*

The effect of alloying elements on two important aspects of massive transformation will be discussed in this section. First is the susceptibility of an alloy to undergo massive transformation, which relates to the ease with which the long-range diffusion process can be stopped in the alloy system so that a transition can be made to the "partitionless" massive transformation. The susceptibility for transformation of α to γ_m is determined by the critical cooling rate for the transformation, that is, the minimum cooling rate that can induce massive transformation in the alloy. The second important aspect is the rate of transformation, which is defined as the amount transformed per unit time and is dependent on the nucleation and growth rates. Growth of massively transformed product is generally accepted to be very rapid and the rate of transformation is governed mainly by the rate of nucleation of γ_m.

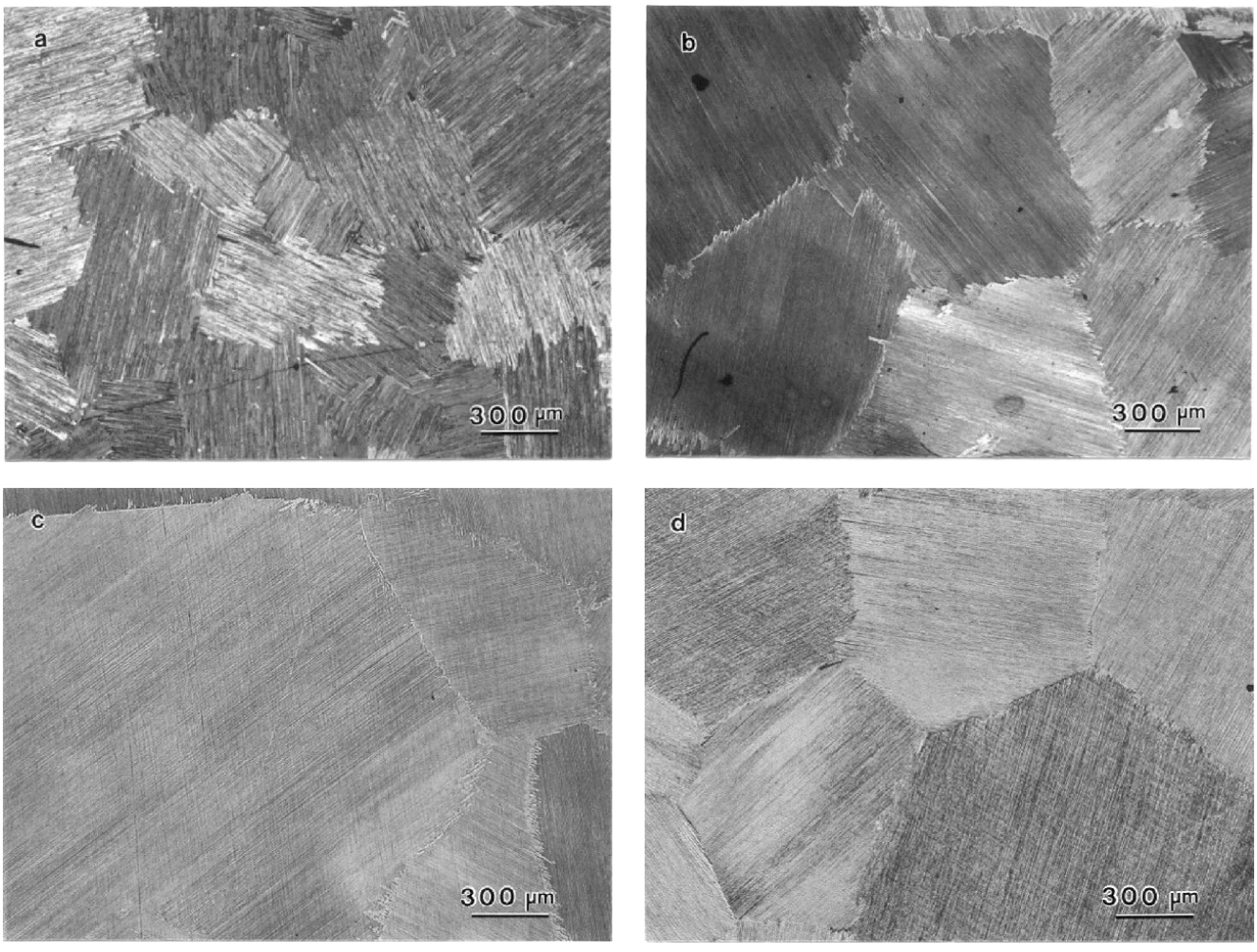

Fig. 4—Optical micrograph showing microstructure obtained in (*a*) alloy I, (*b*) alloy II, (*c*) alloy III, and (*d*) alloy IV, after annealing at 1350 °C for 30 min followed by furnace cooling.

Table II. Variation of Grain Size with Composition

Alloys	Grain Size (μm)
45-2-2 (alloy I)	500
45-2-0.4 (alloy II)	850
45-2-0 (alloy III)	1125
45-0-0 (alloy IV)	980

1. *Susceptibility*

Massive transformation has been observed in the past in various TiAl-based alloys of composition ranging from 46.5 to 49 at. pct Al, with and without the presence of alloying elements.[6–20] It was also suggested by Jones and Kaufman[27] that massive transformation does not take place in the binary Ti-45Al alloy and is favored when the overall alloy composition is close to the equilibrium composition of the gamma phase. The binary Ti-45Al alloy used in their investigation underwent complete alpha to alpha-2 ordering transformation when quenched into ice water from the alpha phase field and massive transformation was observed only in Ti-48Al alloy. Massive transformation, however, was observed in Ti-45Al binary alloy (alloy IV) in the present investigation. One important condition to consider here is the oxygen concentration of the two alloys because it can significantly affect the transformation. Oxygen stabilizes the alpha-2 phase and the implication of this could

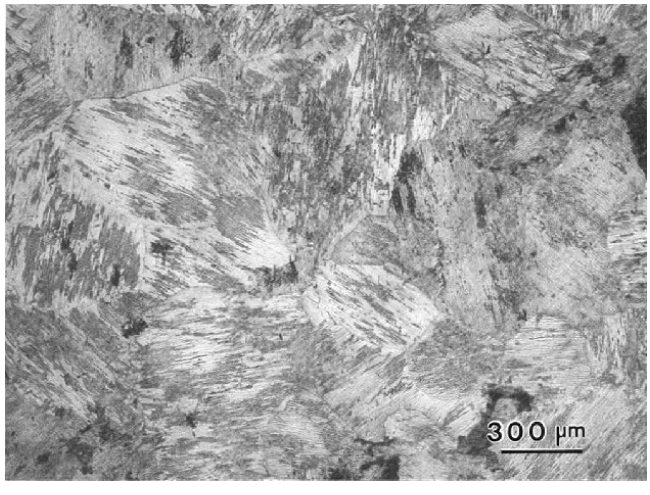

Fig. 5—Optical micrograph showing the microstructure of the air-cooled sample of alloy I.

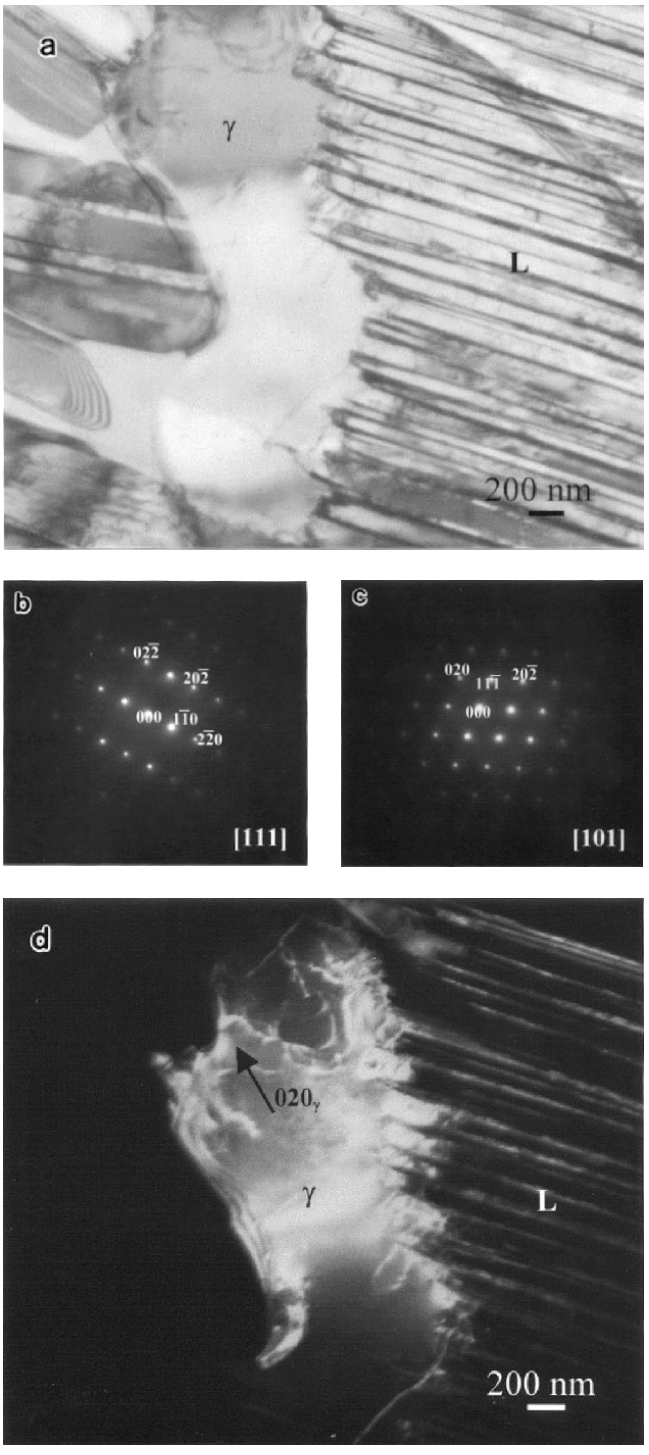

Fig. 6—(*a*) TEM bright-field image showing fine lamellae and blocky gamma phase in air-cooled sample of alloy I. SADPs corresponding to (*b*) [111] and (*c*) [101] zone axes of the gamma phase. (*d*) TEM dark-field image taken with g ~ (020) and *B* ~ [101] confirming the presence of gamma phase.

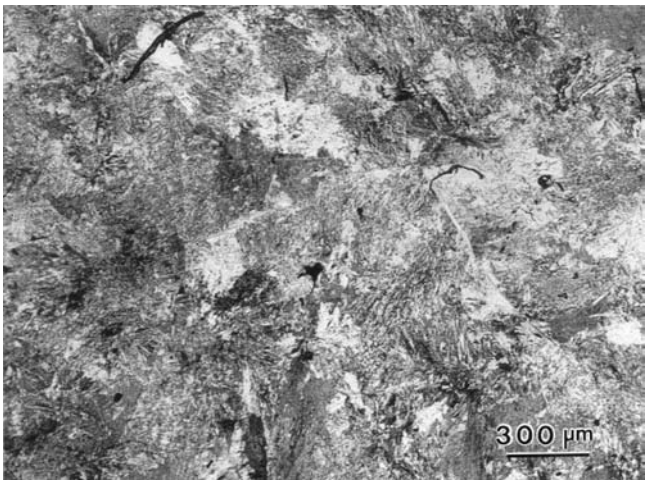

Fig. 7—Optical micrograph showing the microstructure of the air-cooled sample of alloy II.

be the suppression of massive transformation. The oxygen concentrations in the two alloys however, were comparable, *i.e.*, 400 to 700 ppm in the alloy used by Jones and Kaufman and 450 ppm in the binary alloy used in this study. Moreover, in their investigation, Jones and Kaufman reported that the accuracy of the composition measurement was ±1 pct of nominal composition, which was 45 at. pct. This suggests that the composition of the alloy used could have been in the range of 44 to 46 at. pct Al. The microstructural response of the alloy containing less than 45 pct Al is expected to be significantly different from that of the alloy containing 45 at. pct or more Al. Also, the cooling rate experienced by the sample during quenching was not quantified. The binary alloy used in the present investigation contained 45.5 at. pct Al. Based on the results obtained in the present investigation, the CCT diagram proposed by Jones and Kaufman therefore, has been modified to incorporate a curve for massive transformation in the schematic CCT diagram for Ti-45Al alloy (Figure 17(a)). According to this modified diagram, upon furnace cooling, the single-phase alpha would transform to a fully lamellar microstructure. Upon air cooling, the cooling rate would be fast enough to partially suppress the formation of lamellar microstructure and bring about massive transformation of α to γ_m. The cooling curve for water quenching passes through a location far left to the $\alpha \rightarrow \alpha + \gamma$ and the $\alpha_2 \rightarrow \alpha_2 + \gamma$ transformation curves. The transformation product in this case was mainly α_2 with a small percentage of massively transformed gamma phase. The massive transformation never proceeded to 100 pct completion in the binary alloy. At lower cooling rates, the lamellar structure formation was predominant, and, at a relatively high cooling rate, the massive transformation was suppressed by the ordering reaction

In the ternary Ti-Al-Nb alloy system, Nb has been reported to preferentially substitute for Ti sublattice sites in TiAl,[22–26] thereby, increasing the equilibrium aluminum concentration of the gamma phase. The alpha-phase field also expands by the addition of Nb. Addition of Nb to the binary Ti-45Al alloy therefore would move the equilibrium composition of the gamma phase, the $(\alpha + \gamma)/\gamma$ phase boundary, away from the average composition of the alloy. It has been suggested[8,27] that in the Ti-Al system, massive-type transformation is favored when the alloy composition is close to the equilibrium concentration of aluminum in the gamma phase. This suggestion was based on the premise that massive

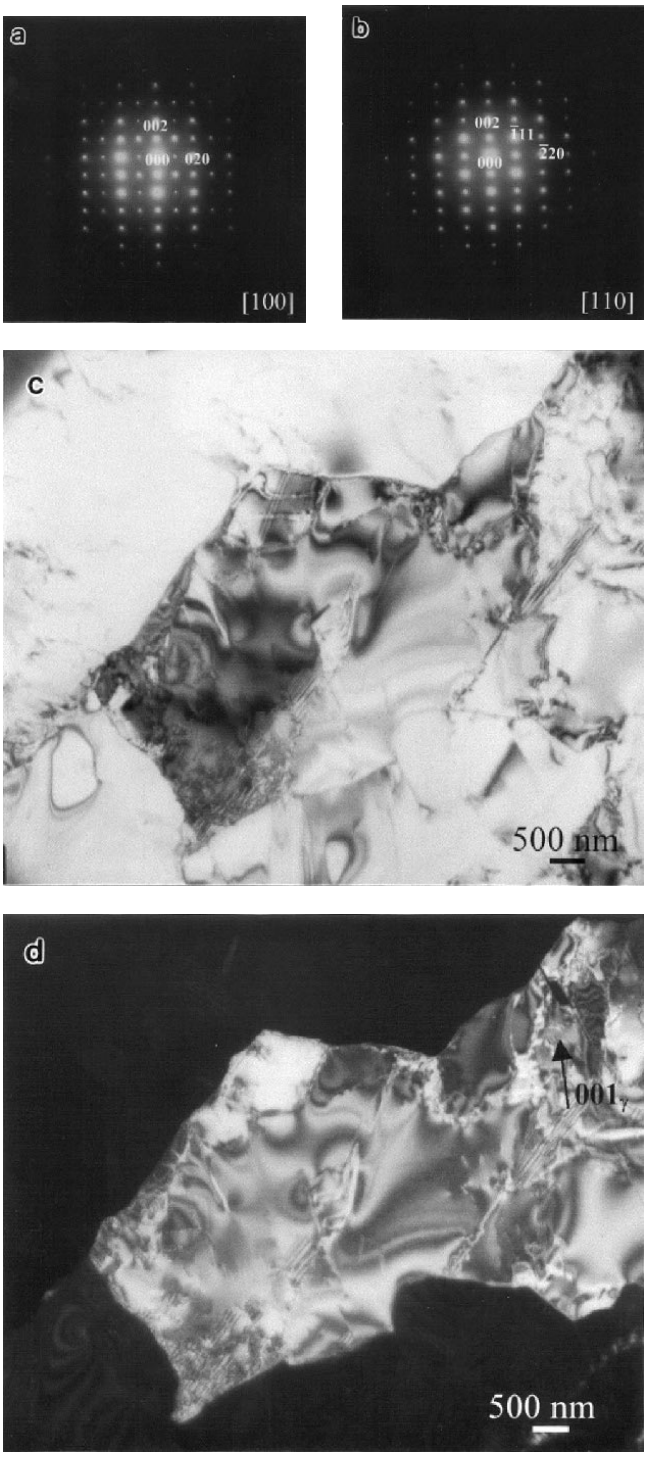

Fig. 8—SADP corresponding to the (*a*) [100] and (*b*) [110] zone axes of gamma in the air-cooled sample of alloy II. TEM (*c*) bright-field and (*d*) dark-field images revealing the presence of massively transformed gamma in the air-cooled sample of alloy II.

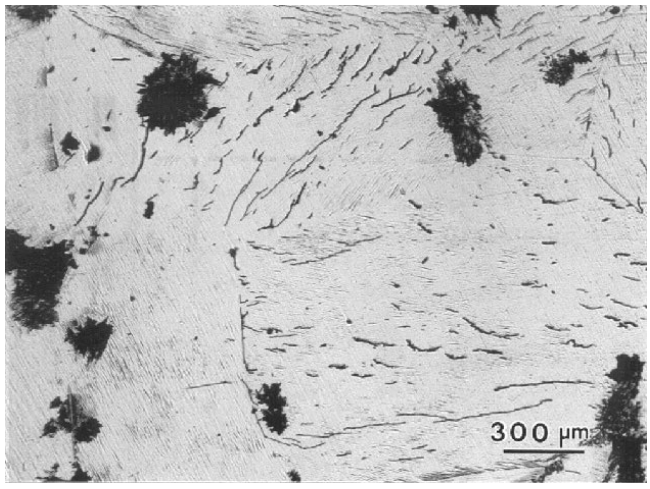

Fig. 9—Optical micrograph showing the microstructure of the air-cooled sample of alloy III.

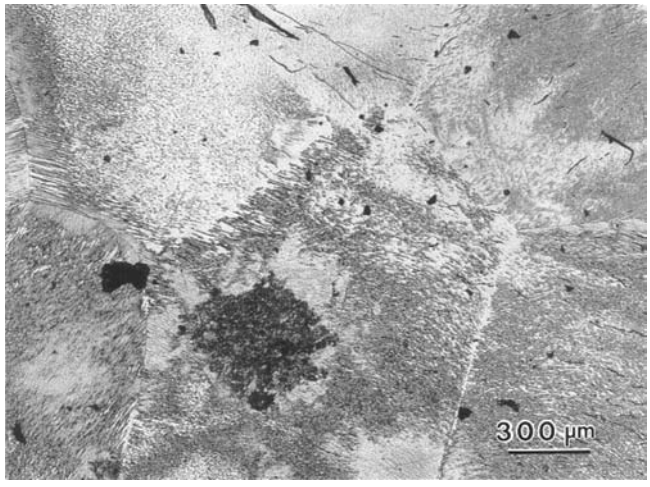

Fig. 10—Optical micrograph showing the microstructure of the air-cooled sample of alloy IV.

transformation was observed in the Ti-48Al alloy but not in the Ti-45Al or Ti-46Al alloy. According to this, addition of Nb to a binary TiAl alloy should reduce the alloy's susceptibility to massive transformation. However, it is important to note that the addition of Nb to a binary Ti-45Al alloy could significantly decrease the diffusivity (Nb being a high melting alloying element), and, hence, at a given cooling rate, it would be easier to prevent long-range diffusion in the ternary alloy with 2 at. pct Nb. As mentioned before, massive transformation is a partitionless transformation and requires a certain minimum cooling rate which is the "critical cooling rate" (CCR) for transformation. This critical cooling rate is required SO as to suppress the diffusion-controlled equilibrium transformation and make the transformation partitionless. The slower the rate of diffusion in a system, the lower will be the value of the critical cooling rate required to prevent long-range diffusion. This explains the observed difference in microstructures between the binary Ti-45Al alloy and the ternary Ti-45Al-2Nb alloy at a cooling rate of ~25 °C/s. The ternary alloy containing 2 at. pct Nb required a relatively lower cooling rate to suppress the formation of lamellar structure and bring about massive transformation, as compared to its binary counterpart. The ternary alloy underwent massive transformation and the microstructure consisted primarily of α_2 phase with small patches of γ_m phase, whereas the lamellar transformation

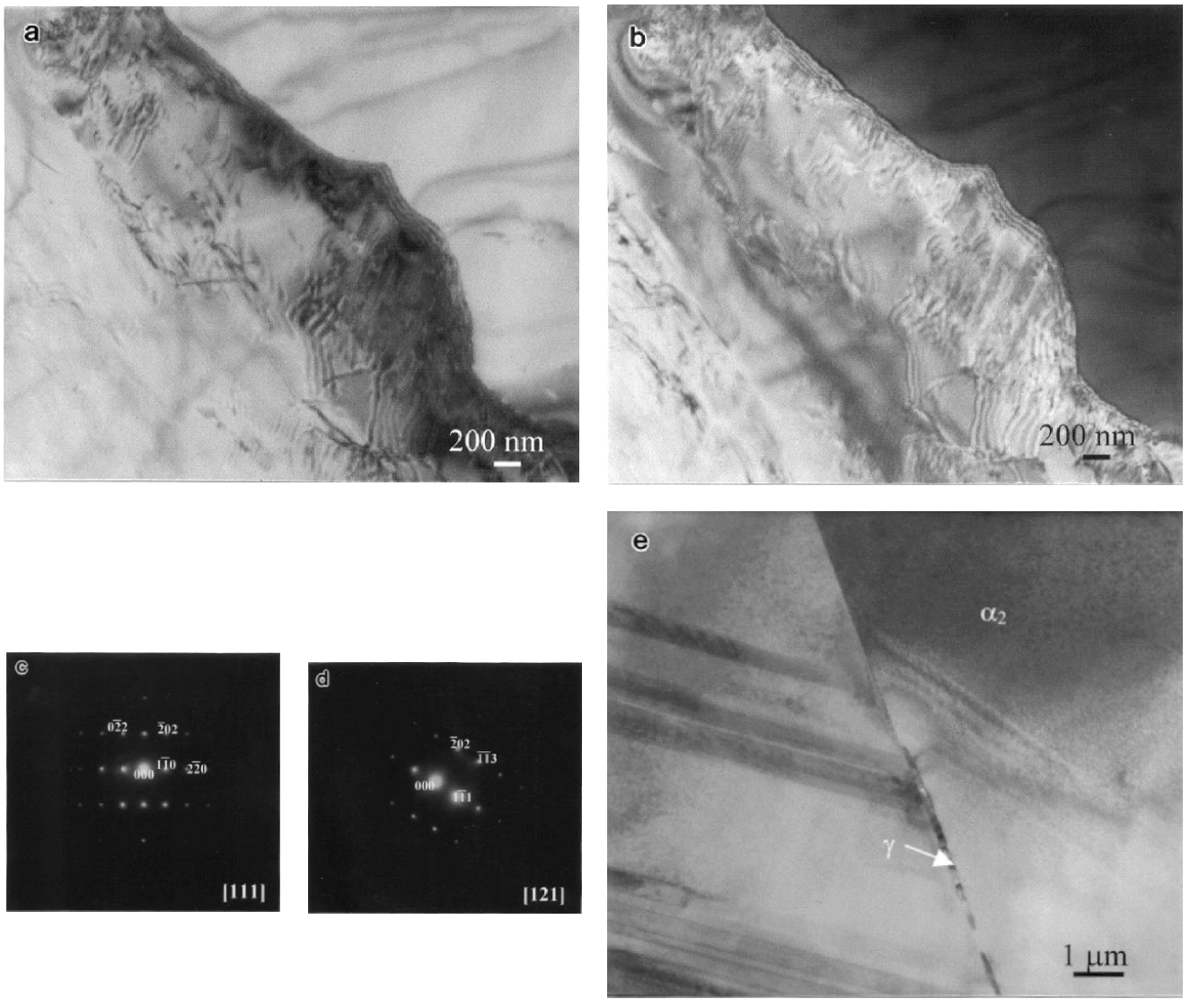

Fig. 11—TEM (*a*) bright-field and (*b*) dark-field image confirming the presence of massively transformed gamma in the air-cooled sample of alloy IV. SADPs corresponding to (*c*) [111] and (*d*) [121] zone axes of gamma phase. (*e*) TEM bright-field image showing the presence of gamma phase at grain boundary in the air-cooled sample of alloy IV.

could not be completely suppressed in its binary counterpart and the resulting microstructure consisted of fine lamellar microstructure along with an occasional presence of massively transformed gamma. Nb is thus suggested to increase the alloys' susceptibility to massive transformation. Upon water quenching, alloy III (Ti-45Al-2Nb) underwent complete ordering reaction, whereas alloy IV (Ti-45Al) consisted of microstructure that was mainly alpha-2 with a small percentage of massively transformed gamma. The CCT diagram for the Ti-45Al alloy shown in Figure 17(a) therefore, has been modified for the ternary alloy with 2 at. pct Nb, as illustrated in Figure 17(b), and is manifested as the shifting of $\alpha \rightarrow \alpha + \gamma$ and $\alpha \rightarrow \alpha_2 + \gamma$ curves to longer times.

In the ternary Ti-Al-Mn system, Mn has been reported to preferentially substitute for the Al sublattice sites in TiAl when present in small concentrations,[24,25,26] thereby reducing the equilibrium Al concentration of the gamma phase. This should bring the overall composition of the alloy closer to the equilibrium composition of the gamma phase, which in turn would tend to favor massive transformation. However, addition of 0.4 at. pct of Mn to the ternary alloy did not alter the susceptibility to massive transformation as much as it did the rate of transformation. A large difference in volume fraction of the massively transformed gamma was observed between the ternary alloy (Ti-45Al-2Nb) and the quaternary alloy with 0.4 at. pct Mn (Ti-45Al-2Nb-0.4 Mn) in AC and WQ samples. This suggests an acceleration of the $\alpha \rightarrow \gamma_m$ transformation by the addition of 0.4 pct Mn. The effect of Mn on the rate of massive transformation will be discussed in detail in Section 2. The effect of the addition of 0.4 at. pct Mn on the CCT diagram is schematically shown in Figure 18(a).

In addition, it should also be noted that Mn is a gamma-phase stabilizer and, it favors the formation of lamellar microstructure. An increase in Mn concentration in the alloy

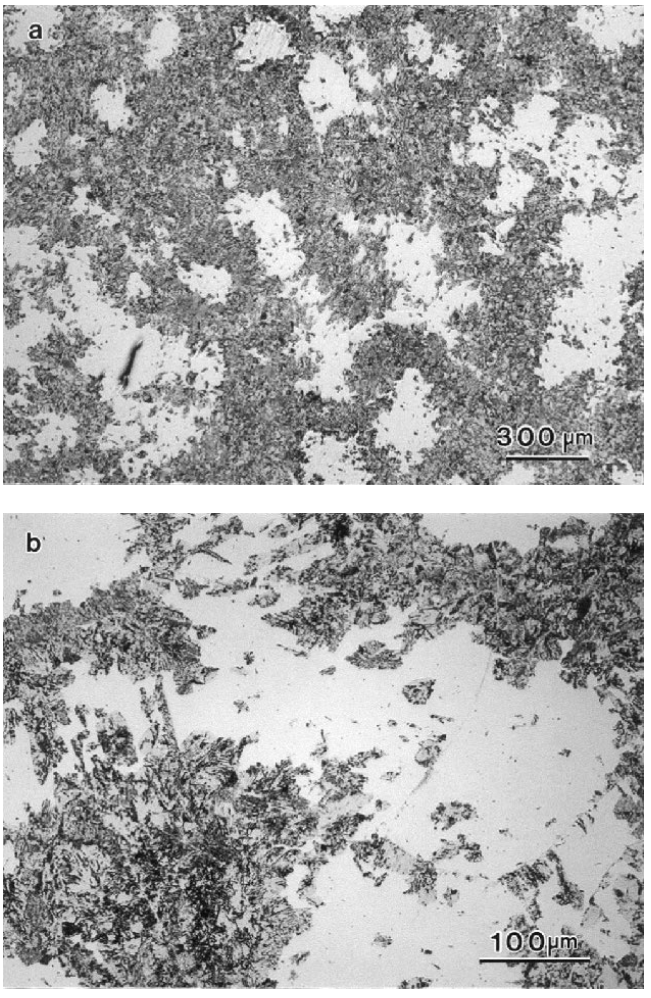

Fig. 12—Optical micrographs showing the microstructure of the water-quenched sample of alloy I ((*a*) 50 times and (*b*) 200 times).

would increase the critical cooling rate (CCR) for massive transformation. An increase in Mn concentration from 0.4 to 2 at. pct indeed decreased susceptibility of the alloy to massive transformation. That is, a much higher cooling rate was required to suppress the transformation of α to the equilibrium lamellar microstructure in alloy I as compared to alloy II. Air cooling of alloy I resulted primarily in a lamellar microstructure, whereas alloy II transformed to almost 100 pct γ_m. Therefore, it is suggested that an increase in Mn concentration would shift the $\alpha \rightarrow \alpha + \gamma$ transformation curve to shorter times. This modification has been incorporated in Figure 18(b) and is manifested as the shifting of the C-curve for the precipitation of equilibrium gamma phase further left to shorter times. As mentioned previously, Mn has been reported to preferentially occupy Al sublattice sites.[23–26] It is also known that the site preference of Mn in TiAl is sensitive to the Al and Mn concentrations in the alloy.[24,25,26] With an increase in Mn concentration in the alloy, the probability of Mn atoms occupying the Ti sublattice sites increases. Alloys I and II are quaternary alloys containing the same amounts of Al and Nb but having different Mn concentrations. A detailed analysis of the effect of Nb on the site occupancy of Mn in the quaternary TiAl alloy

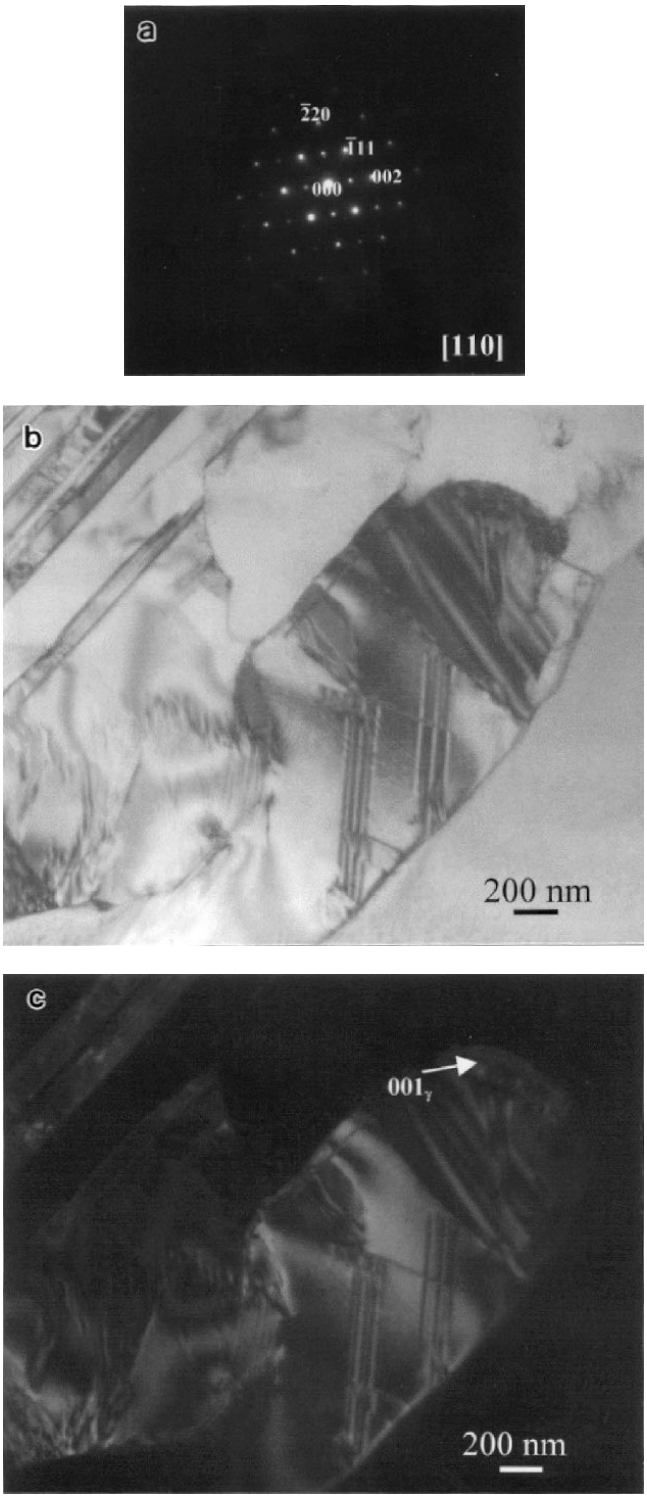

Fig. 13—(*a*) SADP corresponding to the [110] zone axis of the massively transformed gamma phase in the water-quenched sample of alloy I. TEM (*b*) bright-field and (*c*) dark-field image confirming the presence of massively transformed gamma in water-quenched sample of alloy I ($g \sim (001)$, $B \sim [110]$).

is required to comprehensively elucidate the phase transformation behavior in quaternary alloys. The present experimental observations, however, indicate that the addition of Mn to the ternary alloy (Ti-45Al-2Nb) and an increase in

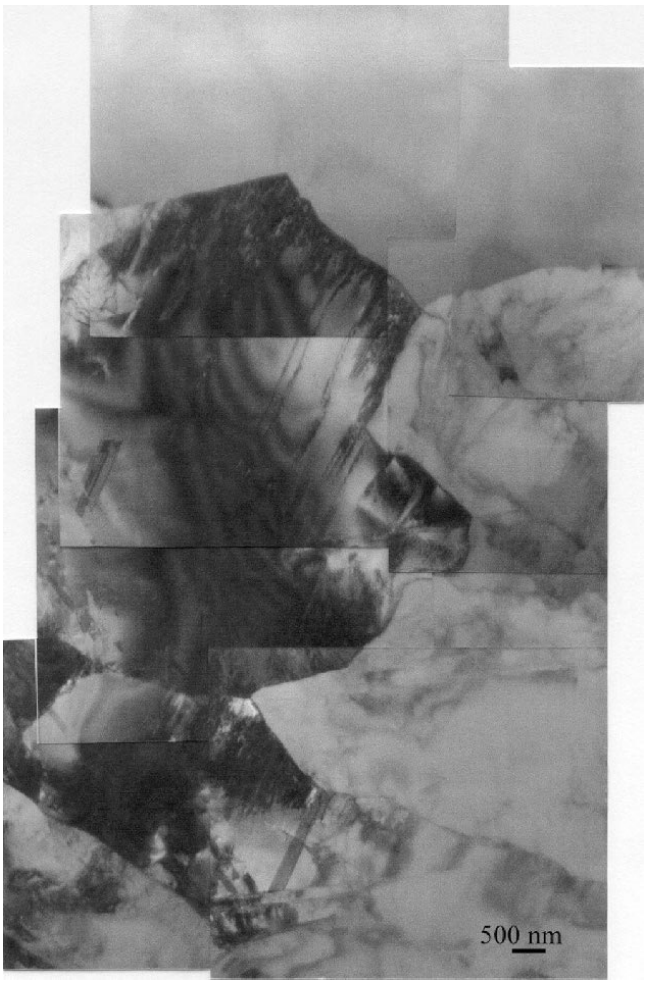

Fig. 14—A collage of TEM bright-field images revealing the overall microstructure of the water-quenched sample of alloy I.

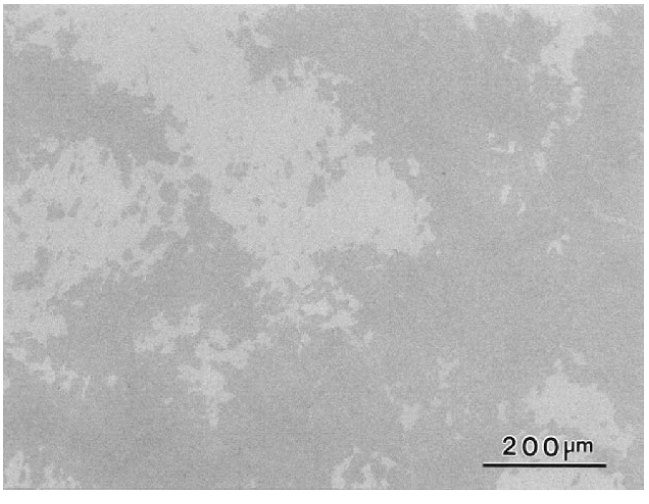

Fig. 15—SEM back-scattered image of the water-quenched sample of alloy I showing weak composition contrast.

Mn concentration caused an increase in the critical cooling rate for massive transformation. This is better illustrated by comparing the air-cooled microstructures of alloys I, II, and III (Figures 5, 7, and 9, respectively). Based on the present results, it appears that perhaps an increase in Mn and the presence of Nb in the alloy reduce the probability of Mn atoms occupying Al sublattice sites. Hence, this supports the suggested effect of Mn concentration on the alloy's susceptibility to massive transformation. Most likely, this is the reason as to why an increase in Mn concentration reduces the alloys' susceptibility to massive transformation.

Table III. Composition of the Product Phases in Water-Quenched Samples

Alloys	Phases	Composition, At. Pct			
		Al	Mn	Nb	Ti
Alloy I	α_2	45	1.5	2	balance
	γ_m	45.5	1.8	2	balance
Alloy II	α_2	45.4	0	2.1	balance
	γ_m	45.4	0.4	1.9	balance

2. *Rate of transformation*

Despite the reduced susceptibility to massive transformation (*i.e.*, an increased critical cooling rate), the volume fraction of massively transformed gamma (γ_m) at a given cooling rate (*viz.* WQ), which was greater than the critical cooling rate, was observed to increase with an increase in Mn concentration of the alloy, as illustrated by a comparison of Figures 12(a) and 16 (a) and (b). As seen in these figures, alloy I, which had the highest concentration of Mn, also had the largest proportion of massively transformed gamma in its microstructure. Also, as seen in Figures 4(a) through (c), the grain size decreased with the increase in Mn concentration in the alloy. The effect of Mn concentration on grain size of fully lamellar microstructure and on the volume fraction of γ_m in water-quenched samples is graphically represented in Figure 19. A larger volume fraction of the massively transformed phase, γ_m, in higher Mn alloy is indicative of a higher transformation rate. This phenomenon can be attributed to the reduction in grain size that accompanies the increase in Mn concentration in the alloy.

It was observed that the addition of Mn reduced the grain size and also made the grain boundaries more irregular and curved. The average grain size was reduced from 1125 to ~500 μm when the Mn concentration increased from 0 to 2 at. pct. The formation of equilibrium lamellar microstructure takes place by the precipitation of gamma lamellae (γ_l) in the pre-existing α grains. The lamellar grains that formed upon furnace cooling after annealing in the α-phase field, hence, are presumed to represent the prior alpha grains. Therefore, it is suggested that perhaps the addition of Mn refines the prior alpha grain size. The exact mechanism of the formation of α grains during supertransus annealing of alloys with fully lamellar starting microstructure is not known. However, it has been suggested that the α phase can nucleate at dislocations, grain boundaries, stacking faults or grain interior during the precipitation of alpha in the gamma phase.[28] Gamma to alpha transformation involves a crystal structure change from ordered fcc to hcp. Introduction of stacking faults into the fcc lattice results in a localized hcp stacking sequence. Hence, stacking faults should be the major nucleation sites for gamma to alpha transformation. Mn is known to reduce

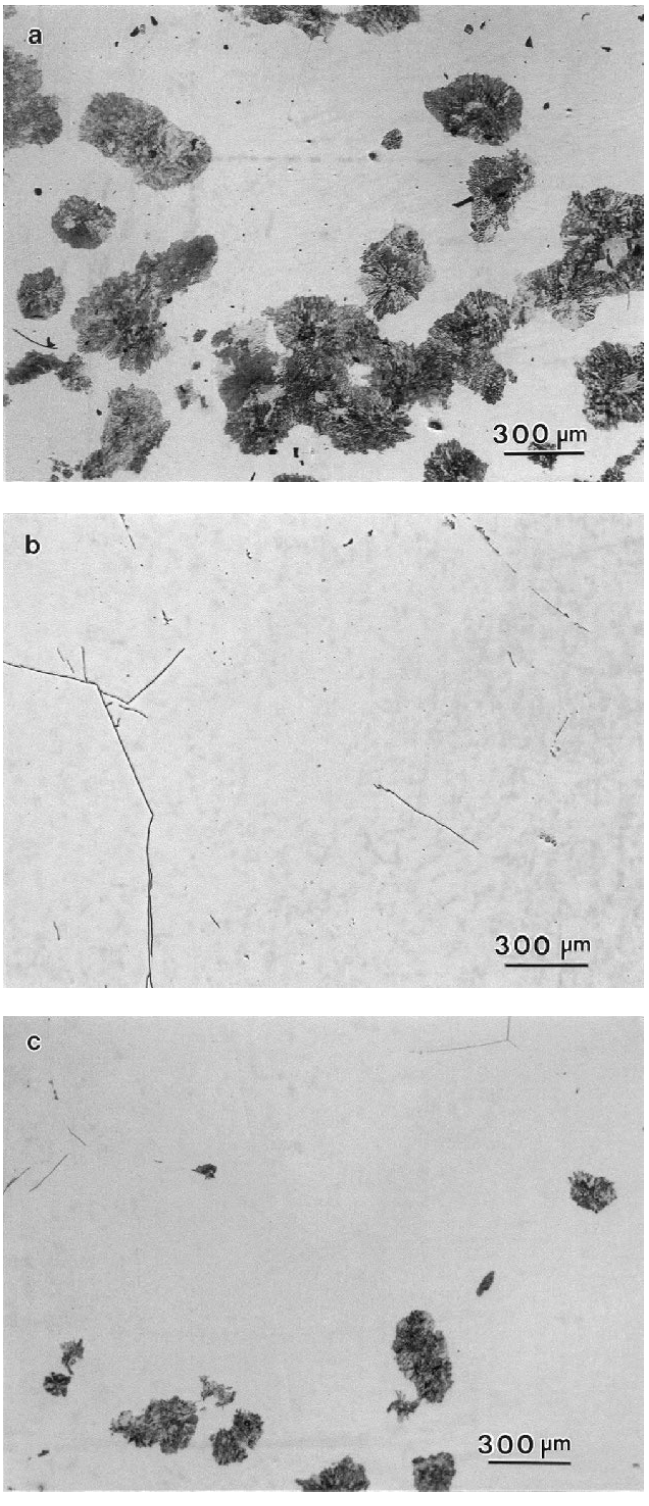

Fig. 16—Optical micrograph showing the microstructure of the water-quenched sample of (*a*) alloy II, (*b*) alloy III, and (*c*) alloy IV.

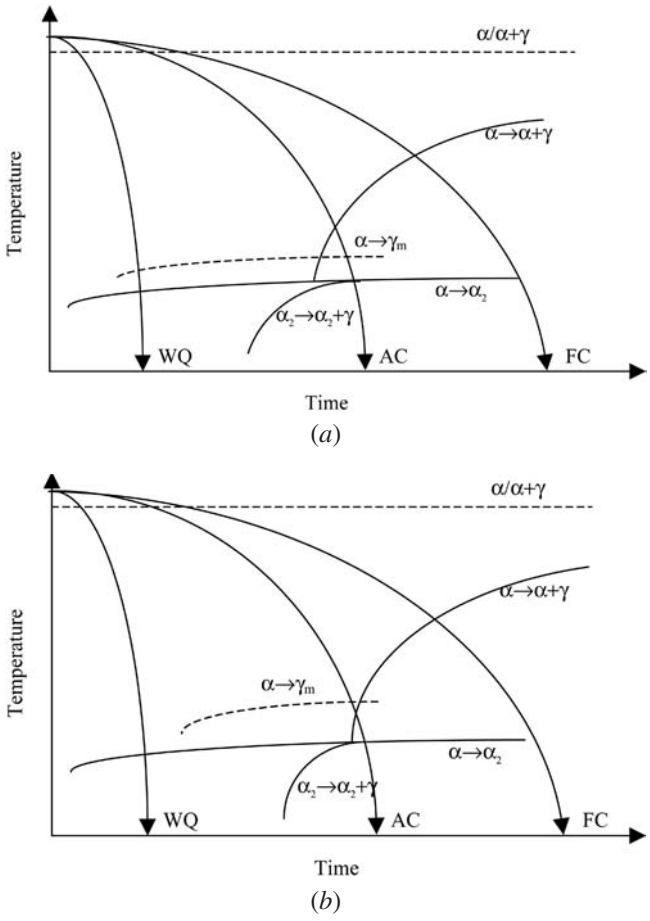

Fig. 17—Schematic CCT diagrams for (*a*) alloy IV (Ti-45Al) and (*b*) alloy III (Ti-45Al-2Nb).

the stacking fault energy in the gamma phase[29,30] and, hence, could result in an increase in the density of stacking faults in the gamma phase. This would increase the nucleation site density for the nucleation of alpha phase. The higher the nucleation site density, the smaller is the size of the product phase. This, perhaps, could be the reason for the reduction in prior alpha grain size with an increase in Mn concentration in the alloy. A decrease in prior alpha grain size would result in an increase in the total grain boundary area per unit volume. This, in turn, would increase the number of sites available for the nucleation of massive gamma at the grain boundaries and, hence, increase the probability of nucleation. This would result in an increase in the rate of nucleation and hence the overall rate of transformation. Also, as seen in Figures 4 (a) through (c), lamellae from one colony penetrated the neighboring colonies across the colony boundaries in higher Mn alloy. These boundaries perhaps have high local internal energy and the energy is minimized by the crossing over of lamellae across these boundaries. These boundaries would also be more favorable for the nucleation of gamma phase and an increase in the area of such boundaries would tend to increase the rate of nucleation. Therefore, it is suggested that addition of Mn enhances the rate of massive transformation kinetics, possibly through altering grain size and grain boundary energy.

The increase in the rate of massive transformation with increase in Mn concentration is manifested as the shifting of the CCT curve for massive transformation to shorter times (Figures 17(a) and (b) and 18(a)). For any nucleation and growth process, the higher the rate of nucleation, the shorter is the incubation period, *i.e.*, the C curve for the

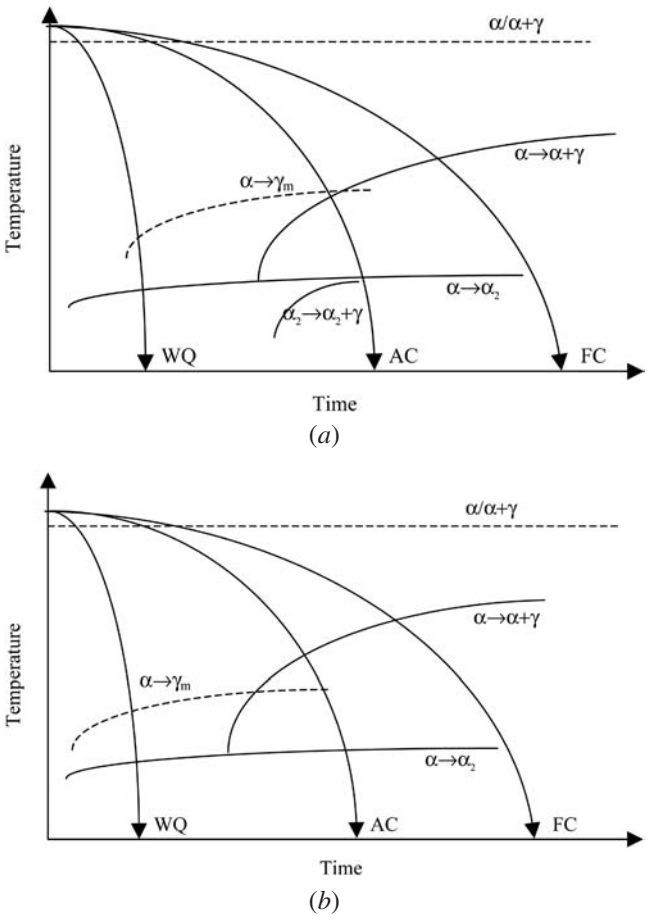

Fig. 18—Schematic CCT diagrams for (*a*) alloy I (Ti-45Al-2Nb-2Mn) and (*b*) alloy II (Ti-45Al-2Nb-0.4Mn).

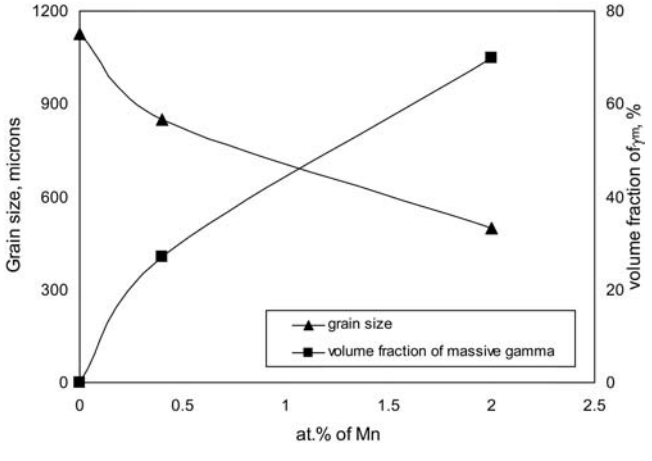

Fig. 19—Plot of lamellar grain size and volume fraction of massively transformed gamma *vs* Mn concentration in the alloy.

transformation moves to the left (*i.e.*, to shorter times). The curve for massive transformation shifts to shorter times with the addition of Mn to the ternary Ti-45Al-2Nb alloy. It was also observed that the volume fraction of γ_m increased with the addition of Mn, which also implies that the rate of massive transformation is accelerated by the addition of Mn. As discussed earlier, this influence of Mn on the rate of massive transformation can be attributed to the reduction in prior grain size in the Mn containing TiAl alloys, which would increase the nucleation rate and, hence, the overall rate of transformation.

E. *Mechanism of Massive Transformation*

One of the issues of major concern regarding massive transformation in the Ti-Al system is its nucleation and growth mechanism. Different mechanisms have been proposed in light of the nature of the interface between the product γ_m phase and the parent α phase.[8,15,17,18] However, no consensus exists regarding these mechanisms. The tentative mechanisms for the nucleation and growth of γ_m are discussed below in Sections 1 and 2.

1. *Nucleation of* γ_m

It was suggested by Denquin and Naka[8] that the nucleation of γ_m phase takes place essentially at the prior α grain boundaries. No rational orientation relationship was observed between the product γ_m phase and the parent phase. Nonetheless, it was proposed that the γ_m phase nucleates at the grain boundary coherently with one grain. They associated the apparent absence of the low index orientation relationship to the experimental difficulties in crystallographically examining the nascent γ_m phase, which they found to be restricted to the vicinity of the α grain boundary. In the present investigation, however, the γ_m phase was found to be present near the grain boundaries as well as inside the prior α grains (Figure 4(b)). Hence, it is suggested that, though the grain boundaries act as primary nucleation sites, the γ_m phase also tends to nucleate well within the interior of prior α grains. Evidence of such intragrain nucleation of γ_m has been also recently reported by Wittig.[31] Careful tilting experiments in TEM during the present investigation also suggested that no specific/rational orientation relationship existed between the parent and the product phase. To definitively establish the nature of the grain boundaries and the inter-phase interfaces, to confirm the mechanism of nucleation for γ_m, comprehensive high-resolution TEM (HRTEM) analysis is required. Nonetheless, based on the results obtained so far, it is suggested here that the γ_m phase primarily nucleates heterogeneously at the prior alpha grain boundaries with occasional nucleation taking place inside the grains.

Zhang *et al.*[15] observed that in a Ti-48Al-2Nb-2Mn alloy the massive gamma phase (γ_m) was always accompanied by the formation of lamellar gamma phase (γ_l). According to their suggested nucleation mechanism, when γ_l intersects a grain boundary, it would propagate into the neighboring untransformed alpha grain in massive manner. This mechanism possibly holds good for higher Al (and higher Mn) alloys in which it is more difficult to suppress the lamellar structure formation. The mechanism for the nucleation of γ_m, proposed by Zhang *et al.*, requires the formation of lamellar gamma phase, which was not the case in this investigation on Ti-45Al- and Ti-45Al-based alloys containing Mn and Nb. It was observed that in rapidly cooled water-quenched samples, a small amount of γ_m phase formed at grain boundaries without the formation of γ_l phase (Figure 11(e)). Therefore, it is suggested that the mechanism for the nucleation of

γ_m, proposed by Zhang *et al*, is not universally applicable to all the TiAl-based alloys, but only to higher Al containing TiAl-based alloys. It is probable that in Ti-45Al based alloys, studied in this investigation, massive transformation of α to γ_m takes place by a mechanism involving heterogeneous nucleation of γ_m at grain boundaries without any specific orientation relationship with either grain.

2. *Growth–nature of growth front and mechanism of γ_m growth*

According to Perepezko[32] and Massalski,[33] the growth of a massively transformed product may be achieved by either of the following two mechanisms: (1) thermally activated short-range jump of atoms across the incoherent interface, in which the interface should be curved; or (2) ledge mechanism, in which the interface should be planar. Both coherent and incoherent interfaces have been previously observed to be present between the massively transformed product and the parent α phase in the Ti-Al system during massive transformation.[8,15,17,18,34] Denquin and Naka[8] reported the γ_m/α interface to be curved. On the other hand, Lin *et al.*[34] reported a completely coherent interface preserving the perfect crystallographic orientation relationship, *i.e.*, $(111)_{\gamma m} // (0001)_\alpha$ and $[110]_{\gamma m} // [11\bar{2}0]_\alpha$ and, hence, suggested a ledge mechanism for the growth of γ_m. Wang *et al.*[17] and Veeraraghavan *et al.*[18] observed both curved and planar interfaces; however, they did not observe any low index rational orientation relationship between the γ_m and α phase. Zhang *et al.*[15] also observed faceted/planar interfaces, but they did not observe any orientation relationship. Based on their results and analyses, both groups have proposed that the γ_m/α interface is incoherent. Many such γ_m/α interfaces were examined in the present investigation in variously heat-treated samples, and both irregular/curved and planar-type interfaces were observed. However, no low index orientation relationship was observed to exist between the parent and product phase. It is therefore suggested that the growth of γ_m seemingly took place by the transfer of atoms across the "incoherent" interface.

Recently, Nie *et al.*[35] have shown that even in the apparent absence of any low-index/rational orientation relationship, the interfaces can be partially coherent rather than completely incoherent. A meticulous HRTEM analysis is required to establish the nature of the interphase interfaces formed under various heat treatment conditions in alloys with varying composition, so that the mechanism of interface migration, *i.e.*, the growth mechanism of γ_m can be ascertained. Nonetheless, based on this study, it is inferred that the product-parent phase interfaces are incoherent in nature and that the growth of massively transformed product takes place by transfer of atoms across these interfaces.

IV. SUMMARY AND CONCLUSIONS

1. Addition of Nb to binary Ti-45Al alloy increased the alloy's susceptibility to undergo massive transformation. An increase in Mn concentration in the alloy, however, resulted in a decrease in its susceptibility to massive transformation.
2. An increase in Mn concentration in the alloy also resulted in an increase in the rate of massive transformation due to its influence on the prior grain size and, hence, on the nucleation rate. An increase in Mn concentration also shifted the C-curve for massive as well as for $\alpha \rightarrow \alpha + \gamma$ lamellar transformation to shorter times.
3. Massive transformation most likely takes place by heterogeneous nucleation at the prior alpha grain boundaries and subsequent growth by short-range transfer of atoms across the "incoherent" interface.

ACKNOWLEDGMENTS

The authors thank the Natural Sciences and Engineering Research Council of Canada and the University of Manitoba for the award of a Graduate Fellowship to one of the authors (UP).

REFERENCES

1. Y.W. Kim: *JOM*, 1994, vol. 46 (7), pp. 30-39.
2. Y.W. Kim and D.M. Dimiduk: in *Structural Intermetallics*, M.V. Nathal *et al.*, eds., TMS, Warrendale, PA, 1997, pp. 531-43.
3. Y.W. Kim: *Intermetallics*, 1998, vol. 6 (7–8), pp. 623-28.
4. C.M. Austin, T.J. Kelly, K.G. McAllister, and J.C. Chesnutt: in *Structural Intermetallics*, M.V. Nathal *et al.*, eds., TMS, Warrendale, PA, 1997, pp. 413-25.
5. S.C. Huang and J.C. Chesnutt: in *Intermetallic Compounds, Practice*, J.H. Westbrook and R.L. Fleischer, eds., John Wiley & Sons Ltd., New York, NY, 1994, vol. 2, pp. 73-90.
6. P. Wang, G.B. Viswanathan, and V.K. Vasudevan: *Metall. Trans. A*, 1992, vol. 23A, pp. 690-97.
7. P. Wang and V.K. Vasudevan: *Scripta Metall. Mater.*, 1992, vol. 27, pp. 89-94.
8. A. Denquin and S. Naka: *Acta Mater.*, 1996, vol. 4 (1), pp. 353-65.
9. E. Abe, T. Kumagai, and M. Nakamura: in *Structural Intermetallics*, M.V. Nathal *et al.*, eds., TMS, Warrendale, PA, 1997, pp. 167-75.
10. M.C. Chaturvedi, N.L. Richards, and Q. Xu: *Mater. Sci. Eng. A*, 1997, vols. A239–A240, pp. 605-12.
11. Q. Xu, M.C. Chaturvedi, and N.L. Richards: *Metall. Mater. Trans. A*, 1999, vol. 30A, pp. 1717-26.
12. X.D. Zhang, T.A. Dean, and M.H. Loretto: *Acta Mater.*, 1994, vol. 42 (6), pp. 2035-42.
13. D. Veeraraghavan and V.K. Vasudevan: in *Gamma Titanium Aluminides*, Y.W. Kim, R. Wagner, and M. Yamaguchi, eds., TMS, Warrendale, PA, 1995, pp. 157-64.
14. Y. Yamabe, M. Takeyama, and M. Kikuchi: in *Gamma Titanium Aluminides*, Y.W. Kim, R. Wagner, and M. Yamaguchi, eds., TMS, Warrendale, PA, 1995, pp. 111-29.
15. D. Zhang, S. Godfrey, M. Weaver, M. Strangwood, P. Threadgill, M.J. Kaufman, and M.H. Loretto: *Acta Mater.*, 1996, vol. 44 (9), pp. 3723-34.
16. T. Kumagai, E. Abe, M. Takeyama, and M. Nakamura: *Scripta Metall. Mater.*, 1997, vol. 36 (5), pp. 523-29.
17. P. Wang, M. Kumar, D. Veeraraghavan, and V.K. Vasudevan: *Acta Mater.*, 1998, vol. 46 (1), pp. 13-30.
18. D. Veeraraghavan, P. Wang, and V.K. Vasudevan: *Acta Mater.*, 1999, vol. 47 (11), pp. 3313-30.
19. U. Prasad, Q. Xu, and M.C. Chaturvedi: *Mater. Sci. Eng. A*, 2002, vols. A329–A331, pp. 906-13.
20. U. Prasad, Q. Xu, and M.C. Chaturvedi: in *Structural Intermetallics*, K.J. Hemker *et al.*, eds., TMS, Warrendale, PA, 2001, pp. 615-22.
21. G. Petzow and G. Effenberg, eds., *A Comprehensive Compendium of Evaluated Constitutional Data and Phase Diagram*, vol. 7 VCH Verlagsgesellschaft, Weinheim, Germany.
22. D.G. Konitzer, I.P. Jones, and H.L. Fraser: *Scripta Metall.*, 1986, vol. 20 (2), pp. 265-68.
23. E. Mohandas and P.A. Beaven: *Scripta Metall.*, 1991, vol. 25, pp. 2023-27.
24. Y.L. Hao, D.S. Xu, Y.Y. Cui, R. Yang, and D.Li: *Acta Mater.*, 1999, vol. 47 (4), pp. 1129-39.
25. Y.L. Hao, R. Yang, Y.Y. Cui and D. Li: *Acta Mater.*, 2000, vol. 48, pp. 1313-24.
26. C. Woodward, S.A. Kajihara, S.I. Rao, and D.M. Dimiduk: in *Gamma Titanium Aluminides*, Y.W. Kim, D.M. Dimiduk, and M.H. Loretto, eds., TMS, Warrendale, PA, 1999, pp. 49-58.
27. S.A. Jones and M.J. Kaufman: *Acta Metall.*, 1993, vol. 41 (2), pp. 387-98.

28. W.J. Zhang, G.L. Chen, and E. Evangelista: *Metall. Mater. Trans. A*, 1999, vol. 30A, pp. 2591-98.
29. M. Morinaga, J. Saito, N. Yukawa, and H. Adachi: *Acta Metall.*, 1990, vol. 38 (1), pp. 25-29.
30. S.G. Pyo and N.J. Kim: in *Gamma Titanium Aluminides*, Y.W. Kim, R. Wagner, and M. Yamaguchi, eds., TMS, Warrendale, PA, 1995, pp. 779-86.
31. J.E. Wittig: *Metall. Mater. Trans. A*, 2002, vol. 30A, pp. 2373-79.
32. J.H. Perepezko: *Metall. Mater. Trans. A*, 1984, vol. 15A, pp. 437-47.
33. T.B. Massalski: *Metall. Trans. A*, 1984, vol. 15A, pp. 421-25.
34. J.G. Lin, C.E. Wen, Y.G. Zhang, and C.Q. Chen: *J. Mater. Sci. Lett.*, 1999, vol. 18, pp. 927-29.
35. J.F. Nie, B.C. Muddle, T. Furuhara, and H.I. Aaronson: *Scripta Metall. Mater.*, 1998, vol. 39 (4–5), pp. 637-45.